Numerical Simulation of Tsunami Generation (Mathematical Physics and Application of Nonlinear Wave Phenomena)

AUTHOR(S):

Kakinuma, Taro

CITATION:

Kakinuma, Taro. Numerical Simulation of Tsunami Generation (Mathematical Physics and Application of Nonlinear Wave Phenomena). 数理解析研究所講究録 2009, 1645: 14-21

ISSUE DATE:

2009-04

URL:

http://hdl.handle.net/2433/140682

数理解析研究所講究録
第1645巻 2009年 14-21

Numerical Simulation of Tsunami Generation

鹿児島大学工学部　海洋土木工学科　柿沼　太郎（Taro Kakinuma）
Dept. of Ocean Civil Engineering,
Kagoshima University

1. INTRODUCTION

In numerical computations of tsunamis due to submarine earthquakes, we usually assume that the initial displacement of water surface is equal to the permanent shift of sea bottom, after which we start calculation of tsunami propagation using a shallow-water or long-wave model. Similar calculation is performed considering multi segments also when seabed-deformation areas change their location. Tsunamis are, however, generated with time. For example, in case of "creeping", where the seabed deformation proceeds slowly, it is not difficult to imagine that the profiles are different between water surface and sea bottom because of propagation during generation of tsunamis.

Outstanding studies have been done focusing attention mainly to initial profiles of tsunamis under some assumptions. Linear analytical solutions of tsunami generation due to seabed deformation were derived by Sano and Hasegawa (1915), Syono (1936), Ichiye (1950), Takahashi (1942), Momoi (1962), Kajiura (1963), Honda and Nakamura (1951), etc., while a weakly nonlinear solution was shown by Hammack (1973). Hydraulic experiments were also performed by, for example, Hammack (1973) and Matsuyama *et al.* (1995), whose results were compared with those of numerical calculation by Nakayama (1983) and Matsuyama *et al.* (1995), respectively, using boundary element methods with velocity potential. Hwang and Divoky (1970) reproduced the field-scale phenomena of tsunami generation and propagation due to the 1964 Good Friday earthquake through a horizontally two-dimensional model with the shallow-water assumption. Ohmachi *et al.* (2001) used a three-dimensional grid system for computations of water motion, where upwelling currents as sources of tsunami generation were given on the sea bottom.

When a deformation area of seabed has a complex topography and its deformation velocity changes in space-time, the initial tsunami profile, which affects calculation results of tsunami propagation and runup, can be evaluated by considering velocity and pressure fields accurately. In this study several generation processes of tsunamis due to seabed deformation have been numerically simulated without assumptions of hydrostatic pressure and long waves. Moreover, several cases where the uplift area of seabed changes its position are treated in the present paper. Aida (1969) performed horizontally two-dimensional linear calculation to investigate directional characteristics of tsunamis due to a dislocation progressing mainly along the long axis of seabed fault. We target uplift-dislocation movement along the short axis of seabed-deformation area, resulting in tsunami earthquakes or tsunamigenic earthquakes to increase the tsunami potential remarkably.

2. NUMERICAL MODEL

A three-dimensional VOF model, which was named STOC-VF and installed in a numerical simulator to study storm surges and tsunamis, i.e., STOC (Kakinuma and Tomita, 2005), is applied to incompressible-fluid motion. Governing equations are the continuity and Reynolds-averaged Navier-Stokes equations, which are solved with a finite difference method. The Poisson equation on pressure is also solved to evaluate not only hydrostatic but also dynamic pressure. The medium porosity is considered to describe smooth shapes of the sea bottom and structure faces, around which the water velocity can be represented more accurately in numerical computations.

When a seabed uplift or subsidence occurs in very deep water, it is efficient to use numerical cells whose size is larger than the seabed shift or water surface displacement. The numerical model has been improved to take into account temporal change of medium porosity, such that the seabed shift is described by temporal change of porosity inside each cell in the neighborhood of the seabed, while the water surface displacement is evaluated by solving an advection equation of a VOF function, which means that elevations of both sea bottom and water surface can be treated also when their movement stays inside each cell. Accordingly, the grid system is fixed without changing the boundary shape of computational domain throughout numerical calculation of tsunami generation, propagation, and runup.

In the computations of this paper, the initial water is still with air cells on the water surface. All fixed boundaries including the sea bottom and side walls are assumed to satisfy the slip condition. The fluid density is spatially uniform and temporally constant, i.e., $\rho = 1.0\times10^{3}$ kg/m^{3}. The total viscosity ν_e is equal to 1.0×10^{-6} m^{2}/s, where any disturbance of a shorter scale than the cell size is neglected.

3. MODEL VERIFICATION IN UPLIFT CASES

Computational results are compared with the corresponding experimental data obtained by Hammack (1973). The area where $-b \le x \le b$ uplifts uniformly. The uplift shift of seabed, ζ, is given as

$$\zeta(t) = \zeta_0(1-e^{-\alpha t}) \qquad \text{when} \quad t \ge 0, \tag{1}$$

where $\alpha > 0$. The ratio b/h_0 is equal to 12.2, where h_0 is the initial water depth. The following two cases are treated in the x-z plane:

(a) Impulsive motion

$$\zeta_0 / h_0 = 0.2 \quad \text{and} \quad t_c\sqrt{gh_0}\,/b = 0.069, \tag{2}$$

(b) Transitional motion

$$\zeta_0 / h_0 = 0.1 \quad \text{and} \quad t_c\sqrt{gh_0}\,/b = 0.39, \tag{3}$$

where $\zeta(t_c) = 2\zeta_0/3$.

The grid widths Δx and Δy are equal to $0.2h_0$, while Δz is $0.05h_0$, where the number

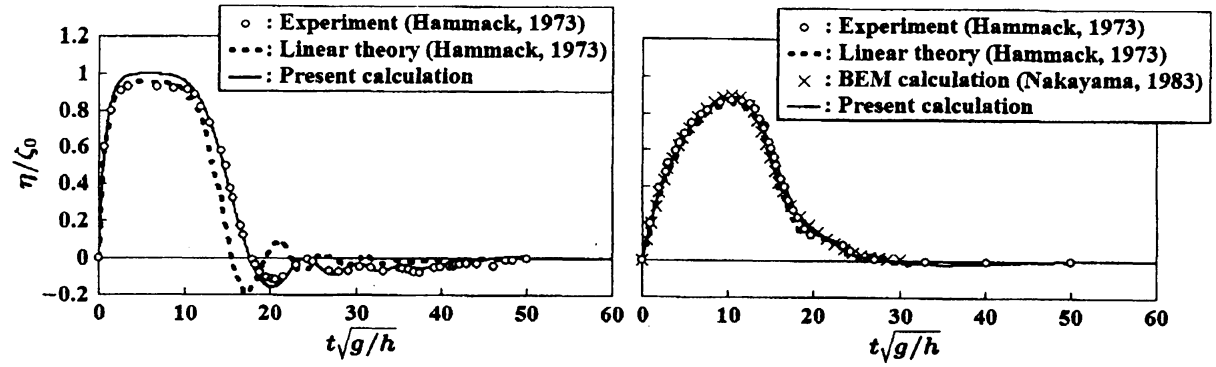

(a) Impulsive motion (b) Transitional motion

Fig.1 Time variations of water surface displacement over the center of seabed-uplift area

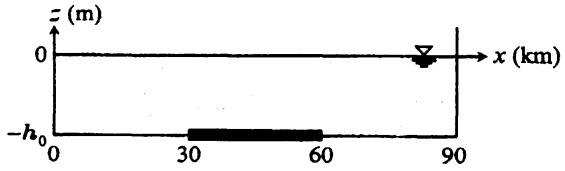

Fig. 2 Definition sketch of calculation domain

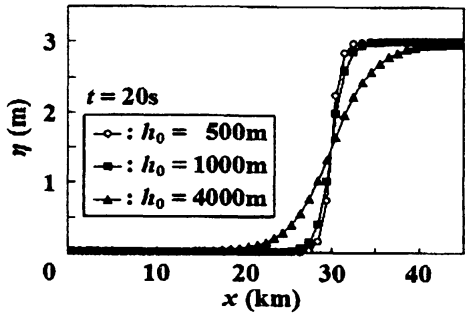

Fig. 3 Initial tsunami profiles, which depend on the initial water depth h_0

of cell along the y-axis is one. The time-step interval changes automatically depending on the Courant number.

The results of water surface displacement over the center of uplift area, where $x/h_0 = 0$, are shown in Fig. 1. In the case of impulsive motion, the present calculation evaluates the water surface displacement accurately, including the short-period oscillations, whose generation should have not only linear but nonlinear mechanisms as well, for the solution of Hammack's linear theory does not show harmony with the experimental data. Also in the transitional motion, the present calculation shows good results, as well as the calculation performed by Nakayama (1983) using a boundary element method (BEM).

4. TSUNAMI GENERATION DUE TO SEABED DEFORMATION WHOSE RISE VELOCITY IS CONSTANT

The calculation domain is shown in Fig. 2. The grid widths Δx and Δy are equal to 1 km, while Δz is 50 m, where the number of cell along the y-axis is one. The time-step interval Δt is equal to 0.5 s.

Figure 3 shows water surface profiles of tsunamis due to a uniform uplift of seabed when t = 20 s, where the initial water depth h_0 is 500, 1,000, or 4,000 m. The seabed deformation occurs inside the area where 30 km $\leq x \leq$ 60 km at the constant rise velocity of

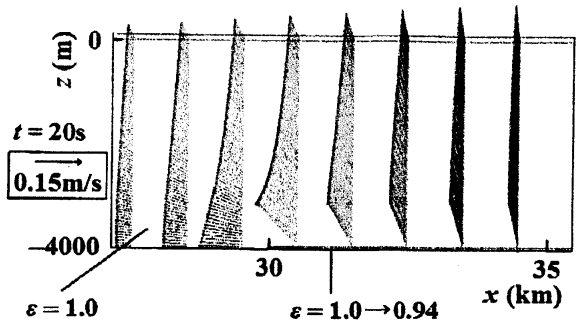

Fig. 4 Water velocity around one end ($x = 30$ km) of the seabed-uplift area

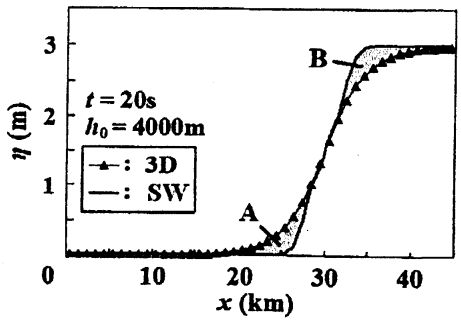

Fig. 5 Initial tsunami profiles, which depend on applied models

0.15 m/s while 0 s$\leq t <$20 s and stops when t = 20 s. In the numerical computations, the porosity of the lowest cells changes from 1.0 to 0.94 inside this deformation area. According to Fig. 3, we can recognize that the "initial profile" of tsunamis, whose generation depends on the initial water depth, is not always the same as the permanent shift of seabed.

Figure 4 shows velocity vectors over the seabed around one end of the deformation area when t = 20 s, where h_0 = 4,000 m. If the water depth is deep in a tsunami-generation area, the horizontal velocity over an edge or a slope of the seabed-deformation area shows a vertical distribution, which cannot be represented through a shallow-water model without dispersion terms.

Figure 5 shows water surface profiles obtained using the present model (3D) and a nonlinear shallow-water model (SW) at the time when t = 20 s. The seabed uplift is the same as that in the cases of Fig. 3. The initial water depth h_0 is equal to 4,000 m. In the calculation with the SW, the temporal derivative of seabed elevation, $\partial z_{\text{bottom}} / \partial t$, is considered inside the seabed-deformation area. In Fig. 5, the water indicated by A, which is evaluated through the 3D, is lifted up to the area B calculated by the SW, such that the SW overestimates the potential energy of initial tsunami. The wave length estimated by the SW is shorter than that by the 3D, resulting in the difference of water surface slope.

5. TSUNAMI GENERATION DUE TO SEABED DEFORMATION WHICH CHANGES ITS OCCURRENCE PLACE

Tsunami earthquakes, which were named by Kanamori (1972) and have been studied by Pelayo and Wiens (1992) etc. mainly in seismology, can generate tsunamis of a larger height than that estimated using only seismic-wave data observed before the tsunamis reach coasts. It is to clear occurring mechanisms of both tsunami earthquakes, which are typified by the 1896 Meiji Sanriku earthquake, and resulting tsunamis that is important for protection against disasters. In this study the seabed deformation due to tsunami earthquakes is classified into the following groups in the view of fluid mechanics through tsunami-generation processes.

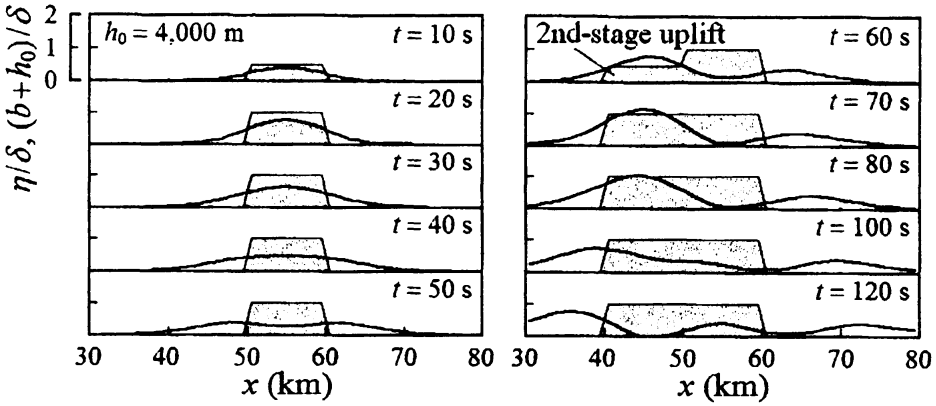

Fig. 6 Time variation of water surface profile due to two-stage uplifts in different areas of seabed. The top faces of gray areas indicate the shapes of seabed. The second stage occurs while $50\ \text{s} \le t < 70\ \text{s}$.

(I) Seabed deformation without interaction with water motion

Type A: Long-duration deformation in a fixed area
Type B: Deformation changing its occurrence place
Type C: Deformation generating water motion affected by surroundings
Type D: Deformation generating significant compression water waves

(II) Seabed deformation with interaction with water motion

Type E: Deformation due to land slides
Type F: Deformation due to inelastic ground movement
Type G: Deformation as extravasation

(III) Seabed deformation with multiple aspects

In order to evaluate seabed shifts and water surface displacements of Types E, F, and G, it is necessary to solve the motion of both sea bottom and sea water simultaneously, for the seabed deformation is interacted with the water motion.

In the present paper, several cases belonging to Type B are treated. The seabed deformation of Type B is subdivided into the following three types.

Type B-1: Multistage deformation in different areas
Type B-2: Deformation changing its occurrence place continuously
Type B-3: Multistage deformation changing its occurrence place continuously in different areas

Figure 6 shows the time variation of water surface profile for a two-stage-deformation case of Type B-1. The seabed inside the area where $50\ \text{km} \le x \le 60\ \text{km}$ uplifts while $0\ \text{s} \le t < 20\ \text{s}$, after which the seabed inside the area where $40\ \text{km} \le x < 50\ \text{km}$ uplifts while $50\ \text{s} \le t < 70\ \text{s}$. The rise velocity of deformation is 0.15 m/s and the permanent shift of seabed,

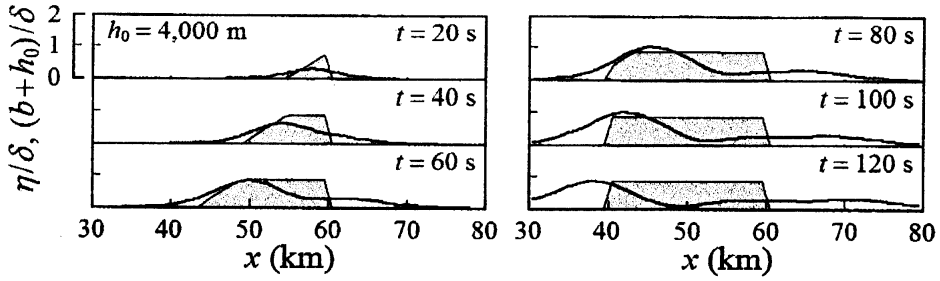

Fig. 7 Time variation of water surface profile due to a seabed uplift changing its occurrence place continuously. The top faces of gray areas indicate the shapes of seabed. The total width of uplift area, R, is equal to 20 km and the progress duration of seabed uplift, τ, is equal to 70 s.

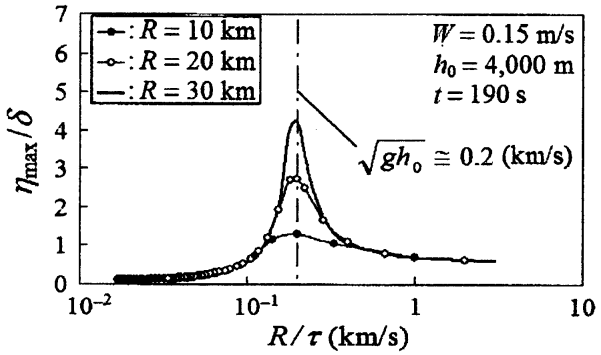

Fig. 8 Relation between height of stably propagating tsunamis, η_{max}, and progress speed of seabed uplift, R/τ. The rise velocity W is equal to 0.15 m/s. The results are shown for cases of different total width of uplift area, R.

δ, becomes 3.0 m. The initial water depth h_0 is equal to 4,000 m. Tsunamis can grow due to succeeding stages inside different areas of seabed deformation. In the present case the almost stably propagating tsunami which has experienced both uplift stages is about twice the height of that in the corresponding one-stage-deformation case when t = 200 s. If there are two areas of dislocation, the tsunami height depends on both place and timing of the second-stage deformation of seabed.

Figure 7 shows the time variation of water surface profile for a case of Type B-2. The seabed-uplift place moves from its start point x_0, where the uplift starts when t = 0 s, to the end point $(x_0 - R)$ $(R > 0)$, where the uplift starts when $t = \tau$ (s), at the constant speed of R/τ. The rise velocity W is equal to 0.15 m/s throughout the seabed-deformation area, after which the uplift stops when the seabed shift becomes 3.0 m, such that the seabed deformation at the end point $(x_0 - R)$ stops when $t = \tau + 20$ s. The initial water depth h_0, the start-point position x_0, the total width of seabed-deformation area, R, and the progress duration of seabed deformation, τ, are equal to 4,000 m, 60 km, 20 km, and 70 s, respectively. In this case the tsunami which propagates towards the negative direction of x-axis at the time when t = 200 s is more than twice the height of that in the corresponding one-stage deformation case, where the seabed-uplift area is fixed, for the seabed-uplift area

chases this tsunami to be effective in growing the wave. On the other hand, the seabed-deformation area escapes from the generated waves traveling towards the positive direction of x-axis, resulting in a narrow width of uplift area which concerns the tsunami growth, while the wave length on this side becomes long.

Figure 8 shows the relation between the wave height of stably propagating tsunamis which have been generated and grown by seabed uplifts of Type B-2, η_{max}, and the progress speed of seabed deformation, R / τ, where the rise velocity W is equal to 0.15 m/s and h_0= 4,000 m. It should be noted that Fig. 8 was obtained using the nonlinear shallow-water model without dispersion terms, i.e., the SW model, although the 3D model was applied to obtain Figs. 6 and 7. The growth rate of tsunamis on the progress sides becomes high especially when the progress speed of seabed deformation, R / τ, is close to the long-wave celerity of tsunamis in the initial water, i.e., approximately $\sqrt{gh_0}$, which is indicated with a dashed line in Fig. 8.

The tsunami height η_{max} depends on both R and τ, as well as W and h_0, such that huge tsunamis, which cannot be predicted using only seismic ground waves, can appear when the seabed deformation occurs due to dislocation of a shallow slide angle or a slow rapture velocity, plastic movement belonging to Type E or F (e.g. Tanioka and Seno, 2001), magma intrusion into sedimentary layers (Kanamori *et al.*, 1993), etc.

6. CONCLUSIONS

Numerical computations of tsunami-generation processes due to seabed deformation in the vertical two-dimension were performed using the three-dimensional model for in-compressible fluids, resulting in accurate initial tsunami profiles, which affect following propagation and runup. The seabed displacement is described by the temporal change of porosity inside numerical cells around the sea bottom, while the water surface elevation is calculated through the VOF method, which means that the present model is able to treat both sea-bottom and water surface elevations also when their change stays inside each cell.

The initial profile of tsunamis, whose generation is dependent on the initial water depth, is not always identical with the permanent shift of seabed. If there are several areas or stages of dislocation, the tsunami height depends on both place and timing of the following-stage deformation of seabed. The growth rate of tsunami on the progress side of seabed deformation becomes high especially when the progress speed of seabed deformation is close to the celerity of tsunami.

Precise analyses of tsunami generation based on fluid mechanics shall contribute to discovery of unheeded types of seabed deformation including those of tsunami earthquakes.

REFERENCES

1) Aida, I. (1969): Numerical experiments for tsunamis caused by moving deformations of the sea bottom, Bull. Earthq. Res. Inst., Vol. 47, pp. 849-862.
2) Hammack, J. L. (1973): A note on tsunamis: their generation and propagation in an ocean of uniform depth, J. Fluid Mech., Vol. 60, pp. 769-799.

3) Honda, H. and K. Nakamura (1951): The waves caused by one-dimensional deformation of the bottom of shallow sea of uniform depth, Sci. Rep. Tohoku Univ., Ser. 5, Vol. 3, pp. 133-137.
4) Hwang, L.-S. and D. Divoky (1970): Tsunami generation, J. Geophys. Res., Vol. 75, pp. 6802-6817.
5) Ichiye, T. (1950): On the theory of tsunami, The Oceanographical Magazine, Vol. 2, pp. 83-100.
6) Kajiura, K. (1963): The leading wave of a tsunami, Bull. Earthq. Res. Inst., Vol. 41, pp. 535-571.
7) Kakinuma, T. and T. Tomita (2005): Development of storm surge and tsunami simulator in oceans and coastal areas, Proc. 29th Int. Conf. on Coastal Eng., ASCE, pp. 1552-1564.
8) Kanamori, H. (1972): Mechanism of tsunami earthquakes, Phys. Earth Planet. Inter., Vol. 6, pp. 346-359.
9) Kanamori, H., G. Ekstrom, A. Dziewonski, J.S. Barker, and S. A. Sipkin (1993): Seismic radiation by magma injection: An anomalous seismic event near Tori Shima, Japan, J. Geophys. Res., Vol. 98, pp. 6511- 6522.
10) Matsuyama, M., M. Ikeno, and H. Tanaka (1995): Proc. 42nd Japanese Conf. on Coastal Eng., JSCE, pp. 226-230 (in Japanese).
11) Momoi, T. (1962): General method of treatment of tsunami caused by the displacement of a portion of the bottom with an arbitrary form, Bull. Earthq. Res. Inst., Vol. 40, pp. 309-324.
12) Nakayama, T. (1983): Boundary element analysis of nonlinear water wave problems, Int. J. num. Meth. Engng., Vol. 19, pp. 953-970.
13) Ohmachi, T., H. Tsukiyama, and H. Matsumoto (2001): Simulation of tsunami induced by dynamic dis- placement of seabed due to seismic faulting, Bull. Seism. Soc. Am., Vol. 91, pp. 1898-1909.
14) Pelayo, A. M. and D. A. Wiens (1992): Tsunami earth- quakes: Slow-thrust faulting events in the accre- tionary wedge, J. Geophys. Res., Vol. 97, pp. 15321- 15337.
15) Sano, K. and K. Hasegawa (1915): On the wave produced by the sudden depression of a small portion of the bottom of a sea of uniform depth, Bull. Cent. Met. Obs. Japan, Vol. 2, No. 3, 30p.
16) Syono, S. (1936): On the waves caused by a sudden deformation of a finite portion of the bottom of a sea of uniform depth, The Geophysical Magazine, Vol. 10, pp. 21-41.
17) Takahashi, R. (1942): On seismic sea waves caused by deformations of the sea bottom, Bull. Earthq. Res. Inst., Vol. 20, pp. 375-400 (in Japanese).
18) Tanioka, Y. and T. Seno (2001): The sediment effect on tsunami generation of the 1896 Sanriku tsunami earthquake, Geophys. Res. Lett., Vol. 28, pp. 3389- 3392.